NUMERICAL MODELLING OF THE NO-CORE-MELT PASSIVE SAFETY FEATURE IN THE GENERATION IV CANADIAN SCWR

Graeme Schmidt[1], John A. Goldak[1], Tarik Kaya[1], Metin Yetisir[2]
[1] Carleton University, Ottawa, Ontario, Canada
[2] Atomic Energy of Canada Limited, Chalk River, Ontario, Canada

Abstract

Heat transfer through a typical fuel channel in a Generation IV Canadian Supercritical Water Reactor was modelled numerically using Finite Element Method software. With the objective of limiting the fuel cladding to sub-melting temperatures during a Loss of Coolant Accident, it was found that two distinct fuel channel designs both attained maximum cladding surface temperatures of approximately T = 1,393 K; a result that compared favourably with the 1,723 K melting point of the stainless steel cladding. The ratios of LOCA to normal operation thermal fluxes were also computed and it was observed that the reference configuration performed best by limiting losses in normal operation while also permitting sufficient heat rejection to the moderator during the LOCA.

Introduction

Canada has been actively involved in the research and conceptual design of Generation IV fission reactors. One of these novel reactor concepts is the SCWR (SuperCritical Water Reactor), which features supercritical water cooling of the Uranium/Thorium fuel [1]. In its current iteration, the Canadian SCWR design features 336 fuel channels (2,540 MW_{th}, 1,200 MW_e total power) immersed in a heavy water moderator [1][2]. Each of these 5 m long fuel channels consist of 64 fuel pins clad in stainless steel, liner tubes (also stainless steel), a ceramic insulator, and a zircaloy pressure tube to contain the assembly. An offshoot of this design, called the SSR (SUPERSAFE© Reactor), employs a scaled down SCWR concept with 120 fuel channels and 300 MW_e total power [3]. These scaled features imply that the thermal energy generated per fuel channel will be similar between the two designs, in turn meaning that the analyses in this paper pertaining to the SCWR are relevant to the SSR as well.

Figure 1 illustrates the operation of a typical HEC (High Efficiency Channel) configuration presented in this paper:

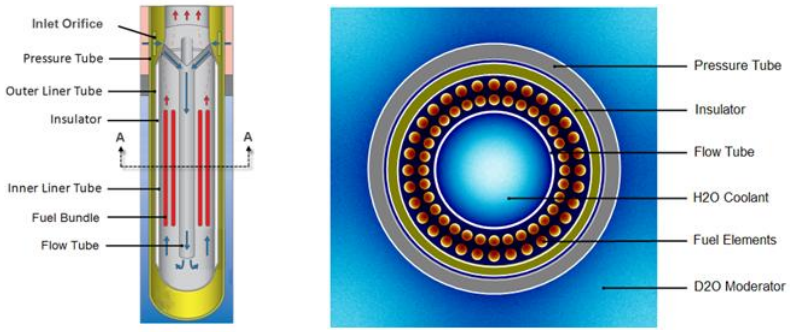

Figure 1: Fuel channel assembly (left) and section view A-A (right). Both graphics courtesy of AECL [2].

With the configuration displayed in Figure 1, coolant temperatures of 623 K and 898 K are achieved at the bottom and top of the fuel channel, respectively, with a constant operating pressure of 25 MPa. On the moderator-side, the heavy-water is maintained at a pressure of 300 kPa and temperature of 353 K via active moderator cooling [4].

During a LOCA (Loss of Coolant Accident), the supercritical water coolant inventory is rapidly depleted and the control rods are subsequently inserted into the core. The resulting radioactive decay of the fission products will continue to generate heat (termed "decay heat") and will cause a rise in temperature in the fuel and its cladding.

To mitigate damage in the event of such an accident, the GIF (Generation IV International Forum) participant nations have resolved to research and implement new safety provisions in next generation reactors. Foremost among these is a passive safety feature, named the "no-core-melt" concept by AECL (Atomic Energy of Canada Limited). In no-core-melt, the decay heat is radiated from the high-temperature fuel cladding to the inner liner, conducted through the other fuel channel components, and is ultimately deposited into the moderator which may serve as an emergency heat sink during accidents. With a proper selection of fuel channel assembly dimensions, it may be possible to reject sufficient decay heat to the moderator such that the fuel cladding is limited to submelting temperatures during a LOCA.

The normal operation and LOCA scenarios described prior were simulated using VrSuite; an FEM (Finite Element Method) multiphysics software package developed by Goldak Technologies Inc© [5]. The software is designed to efficiently solve coupled, transient problems in three spatial dimensions.

1. Methods

Two fuel channel designs were analyzed in VrSuite by way of a 0.5 mm thin cross-section. The governing thermal and stress equations were solved via FEM techniques in three dimensions for both normal operation and LOCA scenarios. During normal operation, heat exchange between the fuel bundle and coolant was modelled using the Dittus-Boelter correlation for forced convection, whereas the net-radiation method was used during the LOCA to simulate radiation heat transfer. Furthermore, thermal conduction across the three expanding/contracting water gaps was computed using fluid properties and gap dimensions updated at each time-step. VrSuite's existing stress solver and a novel radiation solver were coupled with the thermal simulation in order to accurately capture the interacting phenomena. The sections that follow are intended as an in depth description of the methodology summarized above.

1.1 Geometry

Two fuel channel designs (supplied by AECL) were simulated in VrSuite. This was done in order to study the differences in heat transfer characteristics instigated by varying the dimensions of the water gaps, liner tubes, insulator, and pressure tube. A 0.5 mm thin cross-section was analyzed at the top of the fuel channel. Screenshots of the reference geometry may be seen in Figure 2, followed by the dimensions presented in tabular format:

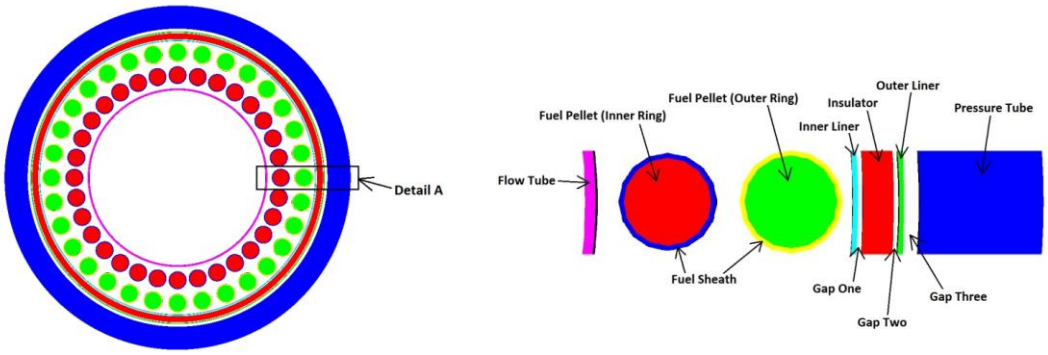

Figures 2: Top view (left) and detail view A (right) of the reference geometry modelled in the VrSuite thermal simulations.

Table 1: Dimensions for the reference and alternate fuel channel designs.

	Reference Design		Alternate Design	
Component	Inner Radius (mm)	Outer Radius (mm)	Inner Radius (mm)	Outer Radius (mm)
Flow Tube	46.0	47.0	46.0	47.0
Inner Liner	72.0	72.5	72.0	72.5
Gap One	72.5	73.0	72.5	72.5
Insulator	73.0	76.0	72.5	72.9
Gap Two	76.0	76.5	72.9	72.9
Outer Liner	76.5	77.0	72.9	73.2
Gap Three	77.0	78.5	73.2	73.7
Pressure Tube	78.5	90.5	73.7	83.7

Table 2: Dimensions for the inner and outer ring fuel pellets and cladding.

	Inner Fuel Ring	Outer Fuel Ring
Pitch Radius (mm)	54.0	66.0
Fuel Pellet Radius (mm)	4.25	4.5
Cladding Thickness (mm)	0.5	0.5

When one considers the temperature difference between the coolant and moderator, it is evident that the radial temperature gradient will be a significant driver of heat transfer through the fuel channel. Specifically, bulk coolant and moderator temperatures of 898 K and 353 K, respectively, yield a radial temperature gradient of 30 K/mm between the inner liner and outer surface of the pressure tube - a length of 18.5 mm.

By comparison, the axial temperature gradient may be considered negligibly small. Specifically, bulk coolant temperatures of 623 K and 898 K at the bottom and top of the fuel channel, respectively, imply an axial temperature gradient of 0.06 K/mm along the 5 m fuel channel length. Consequently, a single cross-section[1] of 0.5 mm axial thickness was simulated at the top of the fuel channel in lieu of the full 5 m length. This simplification was made to circumvent the computational expense associated with modelling the full length of the assembly. The cross-

[1] Although the axial temperature gradient may be considered negligible in this analysis, the VrSuite software by default solves all governing equations in three spatial dimensions.

section was selected at the top of the fuel channel in the interest of conservative design, as the highest coolant temperatures are predicted in this vicinity. However, cross-sections could be selected at any height if desired.

1.2 Governing Equations

The conservation of energy equation governs the time evolution of the thermal fluxes in the solid domain [6][7], as shown:

$$\nabla \cdot q + Q = \rho c_p \frac{\partial T}{\partial t} \quad (W/m^3) \tag{1}$$

Where q is the thermal flux conducted through the solid domain (W/m²), Q is a volumetric heat source term simulating thermal energy generated by nuclear fission (normal operation) or decay heat (LOCA) in the fuel pellets (W/m³), ρ is the density (kg/m³), c_p is the specific heat capacity at constant pressure (J/kg·K), T is temperature (K), and t is time (s).

Strain due to thermal and mechanical loads is governed by the conservation of momentum equation [7], as shown:

$$\nabla \cdot \sigma + b = 0 \quad (N) \tag{2}$$

$$\sigma = D\epsilon \quad (Pa) \tag{3}$$

$$\epsilon = [\nabla u + (\nabla u)^T + (\nabla u)^T \nabla u] \backslash 2 \quad (m/m) \tag{4}$$

Where σ (Pa) and ε (m/m) are the stress and strain, b is the body force (N), D is a fourth order tensor that maps the strain to the stress (Pa), and u is the displacement vector (m).

Heat transfer across the three water gaps is governed by four mechanisms [8]:

- Conduction through the water/steam in the gap (Ω_{Cond}).
- Natural/forced convection of the water/steam in the gap (Ω_{Conv}).
- Thermal radiation between the two bounding surfaces (Ω_{Rad}).
- Through the microscopic asperities of two surfaces in physical contact (Ω_{Asp}) [9].

These mechanisms may in turn be expressed as a sum of thermal conductances per unit area to yield the total conductance across the gap:

$$\Omega_G = \Omega_{Cond} + \Omega_{Conv} + \Omega_{Rad} + \Omega_{Asp} \quad (W/m^2 \cdot K) \tag{5}$$

The resulting thermal flux across the gap may then be expressed as shown:

$$q_G = \Omega_G (T^+ - T^-) \quad (W/m^2) \tag{6}$$

Where T^+ and T^- are the temperatures on either side of the water gap (K). As VrSuite currently does not provide user-support for simulating the latter three conductances in Equation (5), only Ω_{Cond} is considered in the analyses described in this paper. This conductance due to conduction across the gap may be expressed as follows:

$$\Omega_{Cond} = \frac{k}{W} \quad (W/m^2 \cdot K) \tag{7}$$

Where k is the thermal conductivity of the interface medium (W/m·K) and W is the width of the interface (m).

However, it is beneficial to consider the magnitudes of the latter three conductances in Equation (5) in order to estimate the amount of error resulting from their exclusion. Regarding the convection term, it was assumed that this heat transfer mechanism would be negligible in comparison with conduction given the small widths of the gaps. Furthermore, it was found that the high conductivity liquid/supercritical water present in the gaps during normal operation elicited a negligibly small ratio of radiative to conductive fluxes. Conversely, the insulating effect of the low conductivity steam during a LOCA implied a comparatively large proportion of radiative heat transfer, in turn suggesting that the discrepancy resulting from the exclusion of Ω_{Rad} may be considerable in this scenario.

The current technique for computing the heat exchange between two surfaces in physical contact has been expanded upon in Section 1.7.1. The requirements for a more rigorous model of the conductance through asperities are discussed in detail in [9].

1.3 Discretization

Each of the fuel channel components detailed in Table 1 were discretized with 256 equally sized 8-node brick elements in the circumferential dimension. The cross-sections of these segments were maintained uniform, with dimensions of 0.5 mm x 0.5 mm. The fuel pins were meshed in a similar manner, albeit with 16 divisions in the circumferential dimension for each pin. A screenshot of the discretized reference fuel channel assembly may be found below:

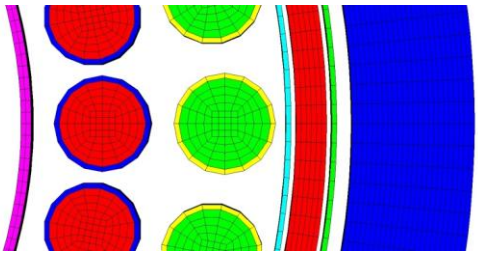

Figure 3: Screenshot from VrSuite depicting the discretized reference geometry.

In addition, the water gaps and interfaces between the fuel cladding and Uranium/Thorium fuel pellets were meshed with contact elements. This was done in order to circumvent the numerical ill-conditioning problems typical of volume elements as their lengths approach zero.

1.4 Fluid/material properties

The relevant water/steam data were compiled from NIST (National Institute of Standards and Technology) [10] and IAPWS (International Association for the Properties of Water and Steam) [11] for pressures of 25 MPa (normal operation) and 100 kPa (LOCA). The dimensionless density, constant pressure specific heat capacity, and thermal conductivity as functions of temperature may be found in Figure 4:

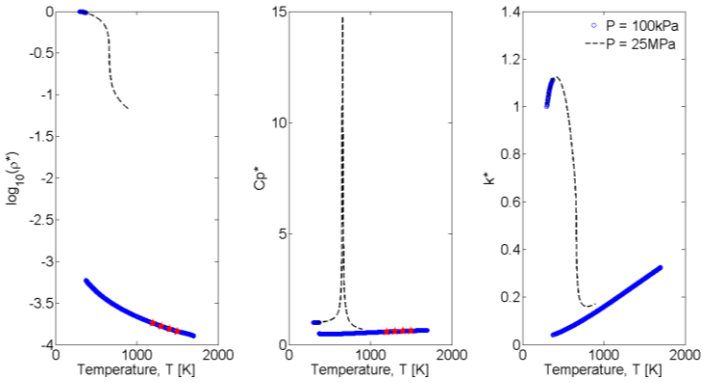

Figure 4: Dimensionless thermofluid properties of water. All data is non-dimensionalized using the properties at T = 300 K.

For 300 K < T < 1,275 K, all fluid property data were acquired from NIST. However, beyond the upper temperature bound, data from NIST were unavailable and MATLAB was used to fit polynomial curves to data from IAPWS (symbolized by red stars in Figure 4). In this manner, extrapolation of the water/steam properties to the necessary 1,700 K was achieved.

Because neither the NIST nor IAPWS websites had conductivity data available for temperatures over 1,275 K, a linear relationship was used to extrapolate beyond 1,275 K to the required 1,700 K. This approach would appear to be valid, as both NIST and IAPWS conductivity values in the vicinity of (but not exceeding) T = 1,275 K are very nearly linearly related to temperature

The data presented above were exported to VrSuite's material library in tabular format. In unison with the computed temperature distributions, the appropriate water/steam properties were extracted from the tables at each time-step for use in calculating the contact conductance across each water gap.

In general, the thermal and mechanical properties of the zircaloy pressure tube, Yttria-stabilized insulator/flow tube, and stainless steel liners/fuel cladding are temperature-dependent. These values, supplied by AECL[2], are as follows:

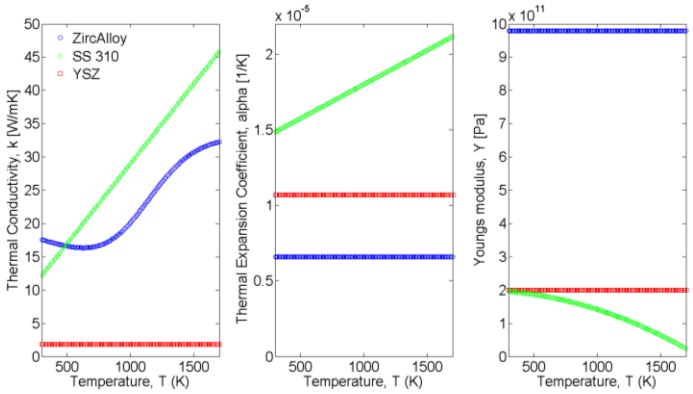

Figure 5: Thermal/mechanical properties as functions of temperature for the fuel channel components.

[2] Verified using independent sources [12][13].

1.5 Initial conditions

The start-up procedure for the Canadian SCWR entails a slow (on the order of 180,000 s [14]) "ramping-up" of the coolant and moderator temperatures/pressures from an initial state to the normal operating conditions detailed in Table 3. However, the steady-state temperature and displacement fields were the only outputs of interest in the normal operation analysis. Thus, a near-asymptotic increase was utilized in the ambient coolant/moderator temperatures from the initial 300 K to the state illustrated in Table 3. This distinction enabled the simulation duration to be compressed from 180,000 s to 400 s.

In addition, a uniform temperature of 363 K was used to initialize the solid domain in normal operation, the rationale for this selection being explained in Section 1.6.1. From the initial conditions illustrated previously, the simulation was permitted to progress to steady-state.

For the LOCA scenario analyses, the steady-state temperature distributions and component deformations under normal operation were used as an initial state.

1.6 Boundary conditions

1.6.1 Thermal analysis – normal operation

The coolant and moderator conditions (for very thin cross-sections near the bottom and top of the fuel channel) during normal operation have been summarized in Table 3:

Table 3: Coolant and moderator conditions near the bottom and top of the fuel channel during normal operation.

	Bottom	Top
Ambient Coolant Temperature	623 K	898 K
Coolant Pressure	25 Mpa	
Coolant Flow Rate	3.9 kg/s	
Ambient Moderator Temperature	353 K	
Moderator Pressure	350 kPa	300 kPa

While all VrSuite simulations were conducted on a cross-section near the top of the fuel channel, the state properties at the bottom were also required in order to estimate the boundary conditions averaged over the full 5 m length of the fuel channel.

In conjunction with the conditions above, the Dittus-Boelter [6] equation was used to estimate the length-averaged heat transfer coefficients at the flow tube (both inner and outer surfaces), fuel cladding, and inner liner:

$$h = \frac{k_c}{D}\left(0.023 Re^{4/5} Pr^{2/5}\right) \quad (W/m^2 \cdot K) \tag{8}$$

Where k_c is the thermal conductivity of the coolant (W/m·K), Re is the Reynold's number (calculated at a characteristic length D), Pr is the Prandtl number, and the diameter D was selected according to the heat transfer coefficient being considered:

- Inner surface of flow tube: D = 92 mm → h = 6,102 W/m²·K.
- Outer surface of flow tube/inner surface of inner liner: $D_h = D_{IL} - D_{FT}$ = (144-94)mm = 50 mm → h = 2,341 W/m²·K, where D_h is the hydraulic diameter, D_{IL} is the inner diameter of the inner liner, and D_{FT} is the outer diameter of the flow tube.
- Outer surfaces of fuel cladding (inner fuel ring): D = 9.5 mm → h = 3,263 W/m²·K.
- Outer surfaces of fuel cladding (outer fuel ring): D = 10 mm → h = 3,230 W/m²·K.

In addition, constant thermal fluxes[3] of q_o = 885 kW/m² and 836 kW/m² were applied to the inner surfaces of the inner and outer fuel ring sheaths, respectively, to simulate heat generated by nuclear fission in the Uranium/Thorium fuel pellets.

Churchill and Chu's correlation [15] for free convection on a vertical wall was utilized at the outside of the pressure tube to simulate heat transferred to the moderator under buoyant action:

$$h = \frac{k_m}{L}\left[0.825 + \frac{0.387Ra_L^{1/6}}{(1+(0.492/\mathrm{Pr})^{9/16})^{4/9}}\right]^2 \quad (W/m^2{\cdot}K) \tag{9}$$

Where k_m is the thermal conductivity of the moderator (W/m·K), L is the length of the fuel channel (m), and Ra_L is the Rayleigh number, defined as follows:

$$Ra_L = Gr_L \,\mathrm{Pr} = \frac{g\beta c_P \rho^2}{\mu k_m}(T_s - T_{\infty,m})L^3 \tag{10}$$

Where Gr_L is the Grashof number, g is the acceleration due to gravity (m/s²), c_P is the constant-pressure specific heat capacity (J/kg·K), ρ is the moderator density (kg/m³), μ is the dynamic viscosity (Pa·s), T_s is the pressure tube surface temperature (K), and $T_{\infty,m}$ is the ambient moderator temperature (K). The moderator volumetric thermal expansion coefficient, β, was expressed in this investigation as follows [16]:

$$\beta(T_f) = -5.51\mathrm{e}^{-5} + 1.22\mathrm{e}^{-6}{\cdot}T_f - 3.99\mathrm{e}^{-8}{\cdot}T_f^2 \quad (°\mathrm{C}^{-1}) \tag{11}$$

Where T_f is the film temperature in °C.

When Equations (9) and (10) are considered, it is apparent that the moderator-side heat transfer coefficient depends strongly upon the outer surface temperature of the pressure tube, both through the Rayleigh number and moderator fluid properties which must be evaluated at the film temperature. Since this pressure tube surface temperature is unknown a priori, the heat transfer coefficient must be re-calculated at each time-step using the surface temperature from the preceding time-step. In VrSuite, this was done by expressing Equation (9) as a polynomial function of the surface temperature, as is shown in Figure 6:

[3] q_o was computed on a "per fuel pin" basis via 2,540 MW_{Th} total reactor power/336 fuel channels/64 fuel pins per fuel channel/fuel sheath surface area.

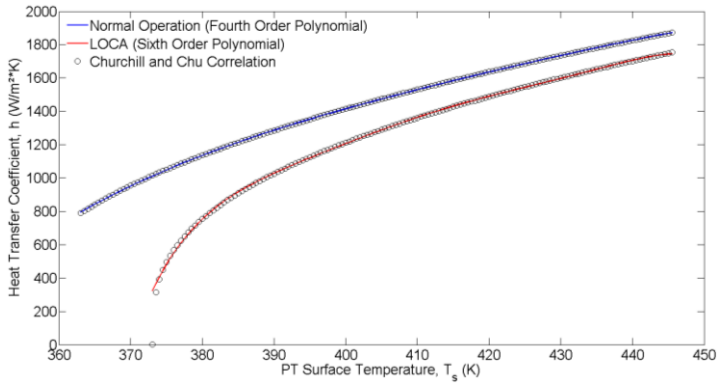

Figure 6: Heat transfer coefficient versus pressure tube surface temperature using Churchill and Chu's correlation. The fitted quartic and sextic polynomials for normal operation and LOCA conditions, respectively, are also shown.

Worthy of note is the seemingly arbitrary selection for the lower temperature bound (i.e. T_s = 363 K for normal operation). While a more intuitive option would be T_s = 353 K, such that $T_s = T_{\infty,m}$ and $Ra_L = 0$, this range yielded a poor fit when compared with that seen in Figure 6. A likely explanation for this poor fit is that the polynomial, regardless of its order, is unable to accurately capture the large changes predicted by Equation (9) in the vicinity of T_s = 353 K. Thus, the entire domain was prescribed a uniform initial temperature of 363 K such that subsequent heat transfer coefficients would closely conform to Equation (9).

While it would be desirable to input Equation (9) into the software in-lieu of an inexact polynomial, this step would require a multitude of subtle, yet complicated alterations to VrSuite's programming.

1.6.2 Thermal analysis – LOCA

In the analyses described as part of this paper, it was assumed that the entire supercritical water coolant inventory was lost at the onset of the LOCA (i.e. at t = 0 s). This implied a consequent cessation of the forced convection illustrated in the last section, in turn meaning that thermal radiation became the sole heat transfer mechanism from the fuel bundle.

The net-radiation method may be used to estimate radiation heat exchange between the discretized surfaces comprising the inner liner, fuel cladding, and flow tube. The governing system of linear equations may be written as follows [17][18]:

$$\sum_{j=1}^{M}\left(\frac{\delta_{kj}}{\varepsilon_j} - F_{k-j}\frac{1-\varepsilon_j}{\varepsilon_j}\right)q_j = \sum_{j=1}^{M} F_{k-j}S\left(T_k^4 - T_j^4\right) \quad (W/m^2) \qquad (12)$$

Where $k \in \{1,2,...,M\}$, M is the number of discretized surface areas comprising the inner liner, fuel cladding, and flow tube, δ_{kj} is the Kronecker-Delta, ε_j is the emissivity of surface element j, F_{k-j} is the view factor between surface elements k and j, S is Stefan-Boltzmann's constant (W/m^2K^4), T_k is the temperature of surface element k (K), and T_j is the temperature of surface element j (K).

Application of Equation (12) to the FEM LOCA thermal simulations necessitated a temperature-independent emissivity for simplicity ($\varepsilon = 0.8$ for all participating surfaces in accordance with the research presented in [19]).

Due to the complex geometry entailed by the 64-pin fuel bundle, the view factors F_{k-j} were computed numerically via the Siemens NX 8.5/TMG© [20] FEM multiphysics software package. The F_{k-j} were then used to compute the thermal fluxes q_j conducted by the participating surfaces. Further details of this process may be found in Section 1.7.1.

The heat generated by radioactive decay of the fission products was modelled as a thermal flux on the inner surfaces of the fuel cladding. The form of this thermal flux was as follows:

$$q(t) = q_o e^{-t/\tau} \quad (W/m^2) \tag{13}$$

Where q_o is the nominal thermal flux calculated in Section 1.6.1, t is the time following the onset of the LOCA (s), and τ is the time constant (calculated to be 0.7024 s by fitting a curve to data from [19]). The exponential decay detailed in Equation (13) was prescribed a start-time of t = 1 s; one second following the onset of the LOCA, wherein a flux of q_o was specified for this duration. This measure was taken to simulate the fuel channel conditions while the control rods are being deployed. The decay dictated by Equation (13) was prescribed from t = 1 s to 2 s, and was in turn followed by a constant heating rate at 7% of q_o.

The moderator-side heat transfer coefficient was estimated in a similar manner as for normal operation, with the ambient moderator temperature being changed to $T_{\infty,m}$ = 373 K. This revised ambient temperature assumes proper functioning of the PMCS (Passive Moderator Cooling System) [4]; a safety feature devised by AECL to ensure that the moderator temperature is maintained below its boiling point in the event of an accident.

1.6.3 Stress analysis

A stress simulation was performed for both normal operation and LOCA conditions, subject to the boundary conditions described in the Figure 7:

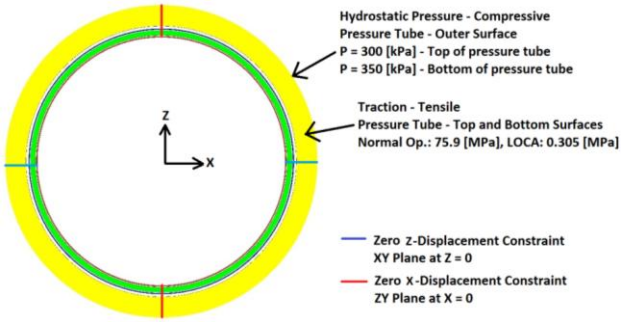

Figure 7: Boundary conditions used in the FEM stress analyses. Unless otherwise stated, a hydrostatic pressure of 25 MPa (normal operation) or 100 kPa (LOCA) acts on every surface. Not shown is the displacement constraint in the Y-dimension imposed upon the bottom surfaces.

Axial traction loads were applied to the top and bottom surfaces of the pressure tube to simulate the hydrostatic pressure of the coolant acting on the end caps of the pressure tube.

1.7 Numerical model

1.7.1 Simulation coupling

As per Equation (12), computation of the net thermal fluxes, q_k, necessitated a known temperature field, T_k. For this purpose, Equations (1) and (12) were coupled together within the VrSuite FEM software. The temperature field from the preceding time-step (i.e. T_k^{n-1}) is used to initialize the radiation solver. With a known temperature distribution, Equation (12) may be solved for the net thermal fluxes q_k^n conducted by the solid domain at the current time-step. These fluxes may then be imposed as boundary conditions on Equation (1), ultimately yielding the temperature field at the current time-step (i.e. T_k^n).

The thermal and stress simulations were also coupled together. By exporting the displacements from the stress solver to the thermal solver at each time-step, the software was able to track the relative motion of the fuel channel components and subsequently calculate the changing gap widths and conductances. The ensuing temperature distribution in the solid domain was then exported back to the stress solver to predict thermal expansion/contraction. It should be noted that physical contact between components is not currently modelled by the software. Therefore, future research might endeavour to simulate this phenomenon (i.e. heat transfer through the mating asperities).

It is conceivable that when the channel components are subjected to large temperatures (and therefore, large thermal strains), two or more of them may come into close proximity. One may recall from Equation (7) that thermal conductance due to conduction exhibits an inversely proportional relationship with the gap width. Thus, in the event that two components do come into close proximity, the thermal conductance may become unbounded (physically, this means the difference in temperatures $T^+ - T^- \rightarrow 0$). To avert this possibility, a "maximum conductance" has been implemented into VrSuite, as is explained in the Figure 8:

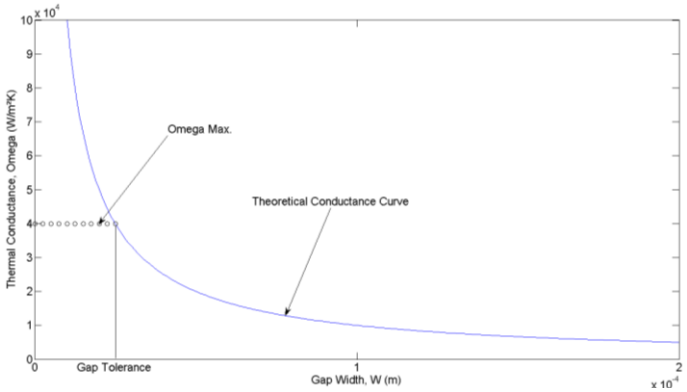

Figure 8: Demonstration of the maximum conductance concept used to avoid unboundedness for thin water gaps.

When the gap contracts to the threshold gap tolerance seen in Figure 8, the thermal conductance is re-assigned the value Ω_{Max} for all deformations with gap width less than the gap tolerance. This allows the simulation to progress without the thermal conductances becoming unbounded.

1.7.2 Simulation parameters

In the normal operation thermal/stress simulations described in this paper, a sufficiently long duration was selected to allow the transient solution to decay to zero, leaving the steady-state temperature and displacement distributions. This selected duration, as well as the resulting global maximum temperature and displacement changes in the final time-step (i.e. $\Delta T_{Max}^{N} = |T_{Max}^{N} - T_{Max}^{N-1}|$ and $\Delta u_{Max}^{N} = |u_{Max}^{N} - u_{Max}^{N-1}|$), have been summarized in the following table:

Table 4: Normal operation analysis duration and temperature/displacement changes at the final (N^{th}) time-step.

Simulation Parameter	Quantity
Duration (s)	400
ΔT_{Max}^{N} (K)	1.13E-03
Δu_{Max}^{N} (m)	1.24E-09

It is apparent from the Table 4 that, when used in conjunction with a time-step of Δt = 1.0 s, the 400 s duration was sufficient to ensure that the normal operation solution attained a steady-state.

The large temperature changes at the onset of the LOCA demanded small time-steps in order to model the transient without succumbing to numerical instability. However, the requirements in the latter stages were less stringent as the solution approached steady-state. Thus, an exponential time-stepping scheme was utilized with the following form:

$$\Delta t^{n} = \Delta t^{1} a^{n-1} \quad (s) \tag{14}$$

Where Δt^{n} is the time-step size at the current (i.e. n^{th}) time-step, Δt^{1} is the time-step size at the first time-step (s), and a is a scaling factor. Parameters of Δt^{1} = 0.1 s and a = 1.01 were used in all LOCA analyses described in this paper.

2. Results and discussion

2.1 Maximum cladding surface temperature

The objective of the no-core-melt concept is to limit the outer surface of the fuel cladding to submelting temperatures in the event of a LOCA. Thus, the reference and alternate design fuel cladding temperatures at the inner fuel ring have been plotted in Figure 9:

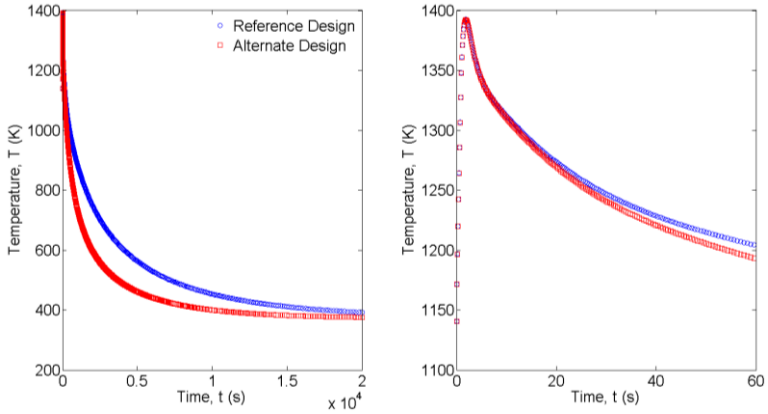

Figure 9: Cladding temperatures over 20,000 s (left) and 60 s (right) LOCA time intervals.

In general, it appears that the alternate design cools to the ambient moderator temperature ($T_{\infty,m}$ = 373 K) at a comparatively faster rate. This pattern likely resulted from the markedly different water gap dimensions between the two variants. For easy reference, these dimensions have been reprinted in the table below:

Table 5: Water gap dimensions for the reference and alternate fuel channel designs.

	Reference Design (mm)	Alternate Design (mm)
Gap One	0.5	0
Gap Two	0.5	0
Gap Three	1.5	0.5

The large temperatures accompanying the LOCA resulted in large thermal strains in the inner liner, meaning that physical contact was made with the insulator in both the reference and alternate fuel channel designs. However, the initially large second and third gaps in the reference design were unable to close over the course of the accident and impeded the flow of heat from the fuel bundle. In the alternate configuration, the third gap was able to close from t = 3 s to t = 246 s, which afforded enhanced heat rejection from the fuel bundle to the moderator. This phenomenon ultimately precipitated the faster cooling rate apparent in Figure 9.

Future research may simulate a circumferentially segmented insulator, allowed to expand and contract freely with the inner and outer liners, in lieu of the monolithic piece studied in this paper. In the alternate fuel channel design, this distinction may allow all three water gaps to close during the LOCA, thus permitting higher rates of heat rejection to the moderator.

From the right-hand plot of Figure 9 it may be observed that the reference and alternate designs yielded global maximum cladding temperatures of 1,392.58 K and 1,392.28 K, respectively, at t = 1.8 s. Both of these results compare favourably with the 1,723 K melting temperature of the stainless steel and support the feasibility of the no-core-melt concept.

However, the similarity in cladding temperatures between the two fuel channel designs (only 0.022% difference) would suggest that the dimensions of the liner tubes, insulator, and pressure tube have little bearing on these results. This trend was most likely prompted by the very short time interval over which the global maximum was attained (i.e. 1.8 s). Over this duration only a small proportion of the radiant heat originating at the fuel bundle is able to propagate to the outer components, in turn meaning that the cladding temperatures during the t = [0,1.8] s interval are nearly invariant with the fuel channel dimensions. Therefore, some other metric is required to ascertain the better performing design.

2.2 Fuel channel efficiency

Efficient fuel channel designs tend to minimize heat loss from the fuel bundle during normal operation while maximizing thermal flux to the moderator during a LOCA. Thus, a convenient metric for performance is a ratio of the LOCA and steady-state normal operation inner liner fluxes, as follows:

$$q^*(t) = \frac{q_{LOCA}(t)}{q_{Normal,S-S}} \tag{15}$$

Where $q_{Normal,S\text{-}S}$ is simply the rate of heat convected from the inner liner by the supercritical water coolant::

$$q_{Normal,S-S} = h(T_{IL,S-S} - T_{\infty,c}) \quad (W/m^2) \tag{16}$$

Where h = 2,341 W/m²·K is the heat transfer coefficient in the annular region between the flow tube and inner liner, $T_{IL,S\text{-}S}$ is the steady-state inner liner temperature, and $T_{\infty,c}$ is the ambient coolant temperature. $T_{IL,S\text{-}S}$ was found to be 877 K and 820 K for the reference and alternate fuel channel designs, respectively.

A plot of q^* as a function of time may be found in Figure 10:

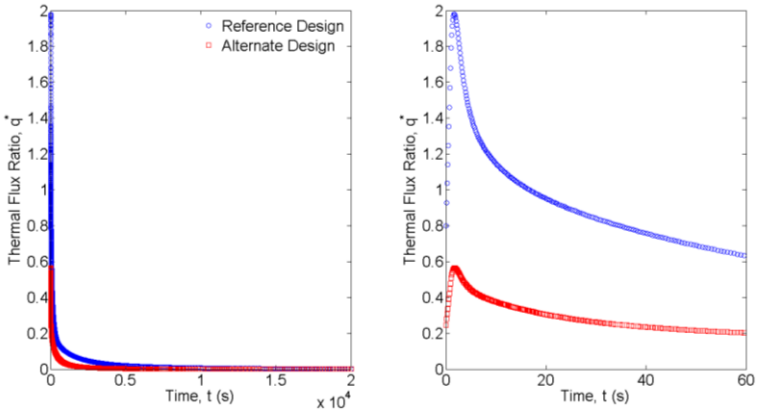

Figure 10: q* for the reference and alternate fuel channel designs over 20,000 s (left) and 60 s (right) LOCA time intervals.

Over the 20,000 s accident duration, Figure 10 would suggest that the reference design performs at a higher efficiency than the alternate, with highly dynamic behaviour being exhibited in the first 60 s. In particular, the reference and alternate designs attained peak efficiencies of q^* = 1.98 and 0.56, respectively, at t = 1.8 s.

The trend described above was likely instigated by the heat transfer characteristics of the water gaps. Specifically, the smaller gaps of the alternate design incurred larger heat transfer rates during the LOCA. However, this favourable consequence came at an expense; these same small water gaps facilitated larger heat losses from the fuel bundle during normal operation. In contrast, the large gaps employed by the reference design evoked a more efficient balance between the LOCA and normal operation thermal fluxes.

3. Conclusions

The objective of the analysis detailed in this paper was to study the heat transfer through a typical Generation IV SCWR fuel channel via FEM techniques. In large part, this goal was achieved by studying the following phenomena:

- Contractions and expansions of the water gaps under combined mechanical and thermal loads, as well as the ensuing changes in thermal conductance across these gaps.
- Radiation heat exchange between the 64-pin fuel bundle, inner liner, and flow tube.
- Variation in heat transfer characteristics elicited by changes in the fuel channel dimensions.

Using the methods enumerated above, the fuel cladding temperatures were calculated as a means of assessing the feasibility of the no-core-melt concept. It was found that the reference and alternate fuel channel designs both yielded sub-melting temperatures of approximately 1,393 K; a result that compared favourably with the 1,793 K melting point of stainless steel.

Given the similarity in cladding temperatures of the two fuel channel designs, it was deemed necessary to use another metric to identify the better performing configuration. In this vein, the ratios of LOCA to normal operation (steady-state) thermal fluxes to the moderator were studied. It was observed that the reference design performed more efficiently by minimizing heat losses from the fuel in normal operation while maximizing heat rejection to the moderator during the LOCA.

In the future, the results presented here for the reference and alternate fuel channel designs may be extended to a larger design space. In this way, it may be possible to identify fuel channel dimensions that attain a state of no-core-melt in the most efficient manner possible. However, further research is required to determine an objective function that best encompasses all of the pertinent merits of such fuel channel designs.

4. Acknowledgements

The authors would like to thank Natural Resources Canada (NRCan) and the National Sciences and Engineering Research Council (NSERC) for their support of the Canadian Generation IV National Program.

5. Bibliography

[1] Leung, L.K.H., Yetisir, M., Diamond, W., Martin, D., Pencer, J., Hyland, B., Hamilton, H., Guzonas, D., and Duffey, R. (October 2011). "A next generation heavy water nuclear reactor with supercritical water as coolant", International Conference Future of HWR's, Ottawa, Ontario, Canada, October 2-5, 2011.

[2] Yetisir, M., Gaudet, M., Rhodes, D., Hamilton, H., and Pencer, J. (August 2014). "Reactor core and passive safety systems descriptions of a next generation pressure tube reactor - mechanical aspects", The 19th Pacific Basin Nuclear Conference (PBNC 2014), Vancouver, British Columbia, Canada, August 24-28.

[3] Yetisir, M., Pencer, J., McDonald, M., Gaudet, M., Licht, J., and Duffey, R. The SUPERSAFE© Reactor: a small modular pressure tube SCWR. *AECL Nuclear Review*. 1:13-18, December 2012.

[4] Licht, J. (March 2013). "Moderator Cooling Requirements for the Canadian SCWR", The 6th International Symposium on Supercritical Water-Cooled Reactors (ISSCWR-6), Shenzhen, Guangdong, China, March 03-07, 2013.

[5] Vr Software Suite. Retrieved from http://www.goldaktec.com/

[6] Çengel, Y. A. *Heat and Mass Transfer - A Practical Approach (3rd Ed.)*. McGraw-Hill Education, 2007.

[7] Goldak, J., Yetisir, M., Pistor, R. (July 2013). "The role of computational weld mechanics in the weld repair of Canada's NRU nuclear reactor", Proceedings of the ASME 2013 Pressure Vessels \& Piping Division Conference (PVP2013-97948)}, Paris, France, July 14-18, 2013.

[8] Goldak, J; Aldea, V; Zhou, J; Wang, S; Mocanita, M; Downey, D; Wang, B. (November 18, 2000). "Coupled Thermal Stress Analysis in Die Casting: A Contact Problem", First M.I.T. Conference on Computational Fluid and Solid Mechanics, Cambridge, Massachusetts, USA, June 12-14, 2001.

[9] Song, S; Yovanovich, M. M.; Goodman, F. O. (August 1993). "Thermal Gap Conductance of Conforming Surfaces in Contact", *Journal of Heat Transfer*, Volume 115, Pg. 533-540.

[10] National Institute of Standards and Technology. Thermophysical Properties of Fluid Systems. Retrieved from http://webbook.nist.gove/chemistry/fluid/

[11] The International Association for the Properties of Water and Steam. Zittau's Fluid Property Calculator. Retrieved from http://thermodynamik.hs-zigr.de/fpc/index.php

[12] International Atomic Energy Agency. (June 2006). "Thermophysical properties database of materials for light water reactors and heavy water reactors", Final report of a coordinated research project (1999-2005).

[13] Schlichting, K.W., Padture, N.P., Klemens, P.G. "Thermal conductivity of dense and porous yttria-stabilized zirconia", *Journal of Materials Science* 36 (2001) 3003-3010.

[14] M. Nimrouzi. A methodology for optimal design of the Canadian SCWR reactor core. M.A. Sc. – Mechanical Engineering, Carleton University, Ottawa, ON, Canada, 2014.

[15] Incropera, Frank P; DeWitt, D (2000). *Fundamentals of Heat and Mass Transfer (4th Ed.)*. John Wiley and Sons, Inc., Hoboken, NJ, USA. 4th edition, 2000.

[16] T.F. Irvine and M.R. Duignan. “Isobaric thermal expansion coefficients for water over large temperature and pressure ranges”. *International Communications in Heat and Mass Transfer*, 12:465-478, 1985.

[17] J. R. Howell, R. Siegel, and M. P. Menguç. *Thermal Radiation Heat Transfer*. CRC Press, Taylor and Francis Group, Boca Raton, FL, USA, 5th edition, 2011.

[18] M. F. Cohen and J. R. Wallace. *Radiosity and Realistic Image Synthesis.* Academic Press Professional, Cambride, MA, USA, 1993.

[19] Licht, J; Xu, R. (April 2012). "Preliminary No-Core-Melt Assessment for the High Efficiency Channel Preconceptual Design", The 3rd China-Canada Joint Workshop on Supercritical-Water-Cooled Reactors, Xi'an, China, April 18-20, 2012.

[20] Maya Heat Transfer Technologies Ltd. *NX 8.5 Thermal Solver TMG Reference Manual*, 2012.